





Measuring an ultrashort, ultraviolet pulse in a slowly responding, absorbing medium

TRAVIS JONES,^{1,2,4}  WILLIAM K. PETERS,¹  ANATOLY EFIMOV,³  DMITRY YAROTSKI,³ RICK TREBINO,² AND PAMELA BOWLAN^{1,5} 

¹Physical Chemistry and Applied Spectroscopy, Los Alamos National Lab, Los Alamos, New Mexico 87544, USA

²School of Physics, Georgia Institute of Technology, Atlanta, Georgia 30332, USA

³Center for Integrated Nanotechnologies, Los Alamos National Lab, Los Alamos, New Mexico 87544, USA

⁴jonetn11@lanl.gov

⁵pambowlan@lanl.gov

Abstract: Frequency-resolved optical gating (FROG) is a common technique for measuring ultrashort laser pulses using an instantaneous, nonlinear-optical interaction as a fast time-gate to measure the pulse intensity and phase. But at high frequencies, materials are often absorbing and it is not always possible to find a medium with a fast nonlinear-optical response. Here we show that an ultrashort, ultraviolet (UV) pulse can be measured in a strongly absorbing medium, using the absorption as the nonlinear-optical time-gate. To do this, we build on our recent implementation of FROG, known as induced-grating cross-correlation FROG (IG XFROG), where an unknown, higher-frequency pulse creates a transient grating that is probed with a lower-frequency, more easily detectable reference pulse. We demonstrate this with an 800 nm reference pulse to characterize 400 nm or 267 nm pulses using ZnS as the nonlinear-optical medium, which is absorptive at and below 400 nm. By scanning the delay between the two UV pulses which create the transient grating, we show that the phase-sensitive instantaneous four-wave-mixing contribution to the nonlinear signal field can be detected and separated from the slower, incoherent part of the response. Measuring a spectrally-resolved cross-correlation in this way and then applying a simple model for the response of the medium, we show that a modified generalized projections (GP) phase-retrieval algorithm can be used to extract the pulse amplitude and phase. We test this approach by measuring chirped UV pulses centered at 400 nm and 267 nm. Since interband absorption (or even photoionization) is not strongly wavelength-dependent, we expect IG XFROG to be applicable deeper into the UV.

© 2021 Optical Society of America under the terms of the [OSA Open Access Publishing Agreement](#)

1. Introduction

The recent development of bright, coherent sources of ultraviolet (UV) to extreme UV (XUV) femtosecond pulses from optical parametric amplifiers, harmonic generation [1], or Free Electron Lasers [2,3] allows for completely new types of time-resolved spectroscopy at higher-energy transitions (e.g. [4–6]), and for pushing any technique to higher spatial and temporal resolutions (e.g. [4,7]). However, to successfully use any of these light sources, whether it is to optimize the light source or for data collection and interpretation, it is necessary to measure the amplitude and phase of the pulses.

Because ultrashort laser pulses are too short to time-resolve with electronics, they are typically measured using a nonlinear-optical interaction as the fast “time-gate” or shutter, since the light-matter interaction can be as fast as attoseconds. This concept is employed in the widely used method of characterizing ultrashort pulses, Frequency-Resolved Optical Gating (FROG) [8]. In a typical FROG arrangement, two or three copies of the pulse to be measured interact in an effectively instantaneously-responding nonlinear-optical medium (e.g. a $\chi^{(2)}$ or $\chi^{(3)}$ interaction)

generating a nonlinear-optical signal which contains a time-gated slice of the unknown pulse electric field, $E_{unk}(t)$. Varying the delay of one of the interacting pulses with respect to the other(s) and measuring the spectrum of the nonlinear-optical signal light generated at each delay produces a spectrogram of the pulse, known as the FROG trace. Conventional phase-retrieval algorithms, such as those based on the method of generalized projections (GP), are used to uniquely reconstruct the complete electric field versus time ($E_{unk}(t)$) of the pulse from the FROG trace. FROG has the added advantage that it can determine the stability of a pulse train [9], and has recently developed improved algorithmic approaches [10–13].

The FROG technique is quite flexible and has been applied in a wide frequency range, from the infrared to the UV. While nearly all FROG measurements have been made using an instantaneous, transparent medium, there are some noteworthy exceptions. In one case, a contribution from a Raman response was accounted for [14]. More recently, FROG was implemented using the fast onset of near-infrared (NIR) induced transient absorption as a time-gate for measuring infrared pulses [15] and plasma mirrors for measuring UV pulses [16]. Similarly, extension of FROG deeper into the UV, where the light-matter interaction is almost always dominated by a long-lived (picoseconds to nanoseconds [17]) transient absorption due to photoexcitation of electrons across the bandgap or photoionization, will require accounting for or using this non-instantaneous response. As a result, most applications of FROG in the deep and extreme UV have bypassed this by relying on the detection of photoelectrons (e.g. [18,19]), rather than having an optical readout.

In this work, we demonstrate that a UV pulse can be measured in a medium that is strongly absorbing using the absorption as the nonlinear-optical time-gate. To do this, we use a novel version of FROG that we recently introduced called Induced-Grating Cross-correlation FROG (IG XFROG) [20]. In IG XFROG, two copies of an unknown UV pulse cross and temporally overlap, creating a transient grating (TG) in a nonlinear medium. A third reference pulse with a different central wavelength, in the NIR, is diffracted from the transient grating to produce a nonlinear-optical signal also in the NIR. Varying the delay between the two UV pulses encodes the intensity and phase of the UV pulse in the NIR nonlinear-optical signal. In this previous work, we introduced IG XFROG as a convenient method for encoding a UV pulse shape in an easily-detectable NIR nonlinear-optical signal. But, so far, we only demonstrated this method in an instantaneously responding, optically transparent medium, restricting its application to lower UV frequencies where an optically transparent medium can be found.

Here, we show that IG XFROG can also be performed in a medium that is *absorbing* at the unknown, UV pulse wavelength. Even a long-lived material response like transient absorption has an initial fast and coherent component [15]. We show that by varying the delay between the UV pulse-pair, it is possible to separate out the fast, coherent part of the material response from the very slow (picoseconds or longer) recovery of the ground state. This results in a nonlinear signal consisting of both an instantaneous, phase-containing contribution and a non-instantaneous, non-phase-containing contribution, but the two contributions can be distinguished and accounted for in the phase retrieval. We demonstrate this by measuring 400 nm and 267 nm chirped pulses in the medium ZnS.

2. Experimental setup

To demonstrate that we can measure femtosecond UV pulses using IG XFROG in an absorbing medium, we built the experiment in the schematic shown in Fig. 1. The light source was a regenerative Ti:Sapphire amplifier at a 1 KHz repetition rate and a center wavelength of 800 nm. A beam splitter (BS1) formed a NIR reference field, E_{ref} , and the UV unknown field, E_{uv} . The unknown UV pulses were centered at 400 nm or 267 nm and were generated by frequency doubling or tripling the 800 nm pulses in BBO crystals. BS2 formed a pair of beams from E_{uv} for generating the transient grating. All three beams were directed to a 250 mm focal length lens which focused and spatially overlapped the beams at the sample, a 2 mm thick ZnS crystal.

The FROG trace was measured as the spectrum of the nonlinear signal versus the delay between the pair of UV pulses, τ_{uv} . For comparison, and to find time-overlap between the three pulses, we also scanned the reference pulse delay, τ_{ref} . Phase-matching was achieved by satisfying the Bragg condition: $\sin\theta_{ref} = (\lambda_{ref} / \lambda_{uv}) \sin\theta_{uv}$. Crossing angles θ_{uv} and θ_{ref} were approximately 1.72° and 3.43° for the 400 nm pulses and 0.747° and 2.24° when measuring the 267 nm pulses.

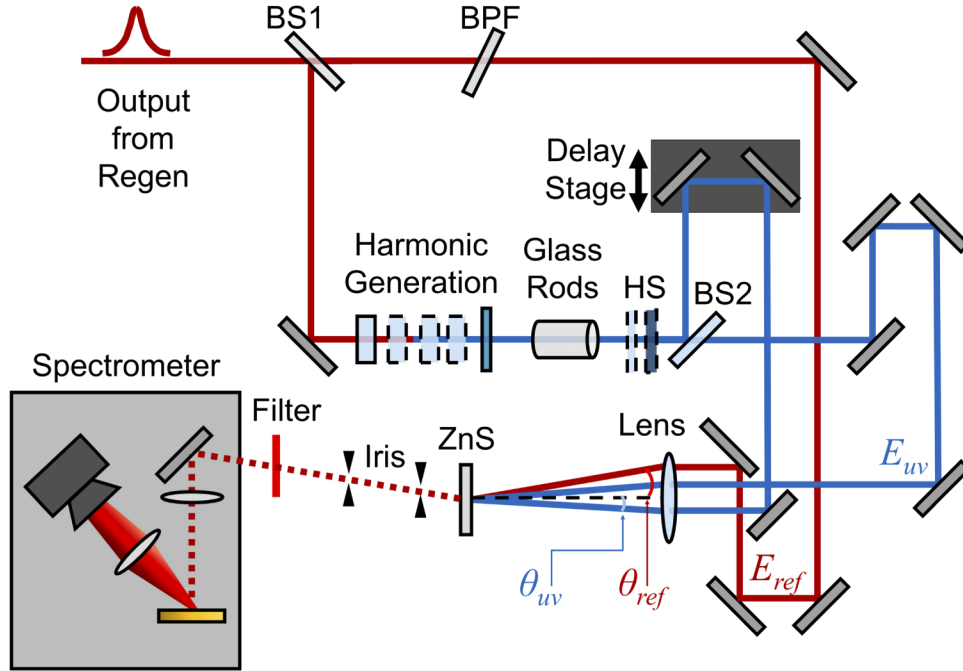


Fig. 1. Experimental setup for Induced-Grating XFROG. 400 nm or 267 nm test pulses were generated by frequency doubling or tripling the 800 nm pulse from a Ti:Sapphire laser system. The 267 nm light was separated from the fundamental and second harmonic light using a harmonic separator and a bandpass filter (HS). Chirped test pulses were measured using glass rods of SF11 or UV-grade fused silica to introduce the chirp. In both experiments, the nonlinear medium was zinc sulfide (ZnS). Phase matching is achieved by satisfying the Bragg condition: $\sin\theta_{ref} = (\lambda_{ref} / \lambda_{uv}) \sin\theta_{uv}$. θ_{ref} and θ_{uv} represent the half-crossing angles for the reference and unknown UV pulses. The half crossing angles for the unknown UV and reference pulses are also labeled accordingly. A 3 nm variable wavelength bandpass filter (BPF) centered at 800 nm was used to spectrally narrow the reference pulse.

To more easily identify phase information in the IG XFROG traces, we found it helpful to spectrally narrow the reference pulse using a 3 nm bandpass filter (BPF). As with any version of XFROG [8,20], IG XFROG requires that the reference field be known and that $E_{ref}(t)$ is an input into the phase-retrieval algorithm. We obtained our reference pulse from a commercial GRENOUILLE measurement which indicated that it was ~ 400 fs long with an approximately flat spectral phase. Having discovered from a reference pulse delay scan measurement that the reference pulse also contained a weak post pulse ~ 850 fs later (outside of the range of our GRENOUILLE), we accounted for this in $E_{ref}(t)$ by adding a second delayed, weaker replica of the main pulse. Accounting for this feature in the reference pulse, which modulates the spectrum of the nonlinear signal, improved the accuracy of the UV pulse retrievals shown later (see Supplement 1 for more details on the reference pulse).

Finally, refractive optics were used, since their dispersion had a negligible effect on the < 2.5 nm bandwidth UV pulses which we considered here. To extend this method to shorter < 50 fs

UV pulses, it would be straight-forward to implement an all-reflective version of the setup shown in Fig. 1 (see for example chapters 13 and 14 in Ref. [8]).

3. Results

3.1. Isolating the instantaneous contribution to the nonlinear signal

Figure 2(a) shows a schematic of the beam geometry used in IG XFROG to measure UV pulses, where two copies of the unknown UV pulse (shown in blue) overlap in space and time such that they induce an interference pattern which modulates the optical properties of the medium, producing a transient grating (TG). There are two major differences here compared to previous TG pulse-measurement techniques [8,21,22]. One is that the grating is generated by the unknown pulse, rather than the reference pulse. This has the major advantage of producing a NIR nonlinear signal, as we pointed out in past work [20]. The second difference is that we scan the delay, τ_{uv} , between the two interfering unknown pulses that create the grating, rather than the delay of the reference pulse, τ_{ref} , which probes the grating. As we also showed in past work [20], varying τ_{uv} is essential for preserving the phase information of the UV pulses, since the nonlinear-optical signal versus τ_{ref} only contains the UV pulse intensity.

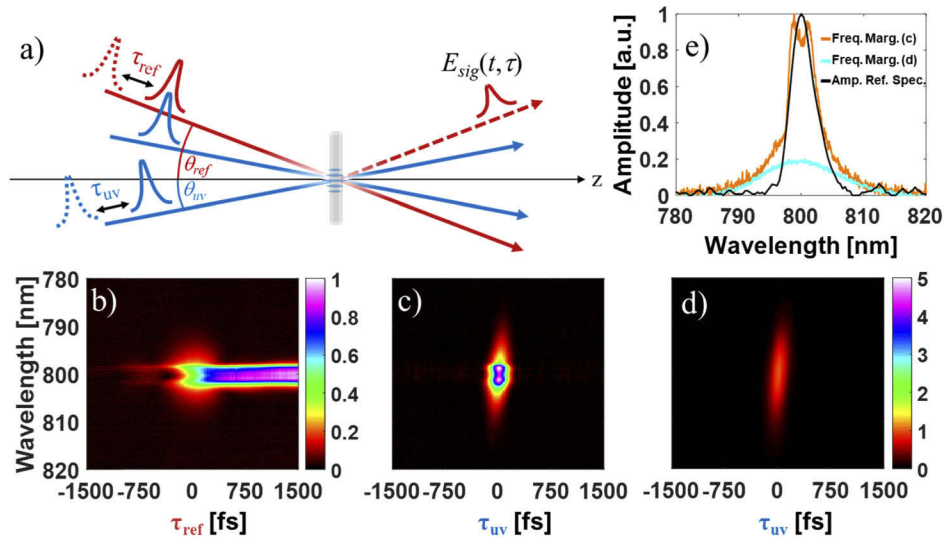


Fig. 2. (a) A schematic of the beam geometry used in Induced-Grating XFROG. The unknown UV, reference, and signal beams are the solid blue, solid red and dashed red lines respectively. Two delays are shown. τ_{ref} is the reference pulse delay and τ_{uv} is the grating-pulse-pair delay. The amplitudes of the traces generated by varying τ_{ref} (b) and τ_{uv} (c) in an absorbing medium (ZnS). (d) The amplitude of the trace for the same measurement as (c), but made using an instantaneous medium (fused silica, see [20]) and rescaled by a factor of 0.2. (e) A comparison of the frequency marginal of (c) (orange) to the frequency marginal of (d) (cyan) and the spectral amplitude of the reference pulse (black). Note that in (b) the nonlinear signal extends well into positive delays, while in (c) the full duration of the signal is shown.

Another major advantage of scanning τ_{uv} in an absorptive medium is illustrated in Figs. 2(b)-(e). Here we used ZnS as the nonlinear medium, which has a nominal bandgap of ~ 3.5 eV, and becomes absorptive at around 400 nm [23]. Figures 2(b) and 2(c) show the amplitude of the spectrally resolved nonlinear signals versus the two different delays. Figure 2(b), shows two distinct features: a spectrally broader component near zero delay and a narrower-bandwidth

long-lived component. The spectrally broader component is suggestive, although not definitive proof, of coherent four-wave-mixing (FWM) (i.e. incoherent optical switching is also possible, which could cut the pulse in time without preserving the phase). This is important since a coherent material interaction is needed to preserve the UV pulse phase information in the signal. The longer-lived component, which persists after the pulses no longer temporally overlap, is the timescale for relaxation of the photoexcited electrons back to their ground state (i.e., the lifetime).

In contrast, a trace versus τ_{uv} in ZnS is shown in Fig. 2(c), which does not show the long-lived response seen in Fig. 2(b). This is because the induced grating, and hence the nonlinear signal, only exists while the UV pulses temporally overlap (to within the material dephasing time [24–27]). Thus, the duration of the nonlinear signal versus τ_{uv} is approximately reduced to the length of a cross-correlation, similar to that reported in [28]. The image in Fig. 2(c) also again suggests a coherent FWM contribution to the signal. This is best seen by comparison to Fig. 2(d), a measurement of the same pulse using UV fused silica as the nonlinear medium, which has an instantaneous and purely coherent FWM response [20]. There is a broader-band component in the ZnS measurement in Fig. 2(c) which matches, both in tilt and bandwidth, to that seen in the fused silica measurement in Fig. 2(d). This suggests that the measurement in Fig. 2(c) does contain the amplitude and phase of the UV pulse.

Still, some dephasing occurs within the UV pulse duration and the image in Fig. 2(c) also has a non-phase-containing contribution: the round, central portion not seen in the fused silica measurement. The bandwidth of this round, central portion matches that of the NIR reference pulse.

3.2. Incorporating the material response into the generalized projection phase-retrieval algorithm

As illustrated above, the FROG trace in Fig. 2(c) contains an instantaneous and a non-instantaneous contribution, both of which need to be accounted for in the phase retrieval. We follow the approach used by Delong *et al.* [14] where polarization gating FROG was done in the presence of Raman effects, resulting in a non-instantaneous contribution to the signal. The nonlinear signal $E_{sig}(t, \tau)$, is treated as a sum of the instantaneous and non-instantaneous contributions. Using an empirical model for the signal field we write:

$$E_{sig}(t, \tau) = E_{ref}(t - \tau_{ref}) \int_{-\infty}^t dt' R(t - t') E_{uv}^*(t') E_{uv}(t' - \tau_{uv}). \quad (1)$$

In the above expression, $R(t)$ represents the response of the medium and is given by,

$$R(t) = \delta(t) + c_{\Theta} \Theta(t), \quad (2)$$

or the sum of a delta function, $\delta(t)$, and a Heaviside step function, $\Theta(t)$, scaled by c_{Θ} to adjust the relative amplitudes of these two terms. In this model, the Heaviside function alone is sufficient for providing a needed fast time-gate as pointed out in previous work using NIR transient absorption as a fast time-gate [15]. Here the delta function has been included to adjust the relative amplitudes of the phase-containing and non-phase-containing contributions, to better match the model to the measurements. To fit the model to the data, we chose the constant empirically, finding that a value of $c_{\Theta} = 5$, typically fit our data sufficiently well. Figure 3 shows an example of a simulation we did to determine $R(t)$. The comparison suggests that the simple model sufficiently captures the material response and can be used for phase retrieval.

To retrieve the UV pulse from our spectrograms, the signal field given by Eqs. (1) and (2) was incorporated into a modified GP phase-retrieval algorithm where the FROG trace is given by $I_{FROG}(\omega, \tau) = |\mathcal{F}[E_{sig}(t, \tau)]|^2$, where \mathcal{F} indicates a Fourier transformation. The algorithm that we used here follows the procedure outlined in [20], where the reference field is a known input, and the derivatives for the nonlinear signal given in Eq. (1) are used in the gradient minimization.

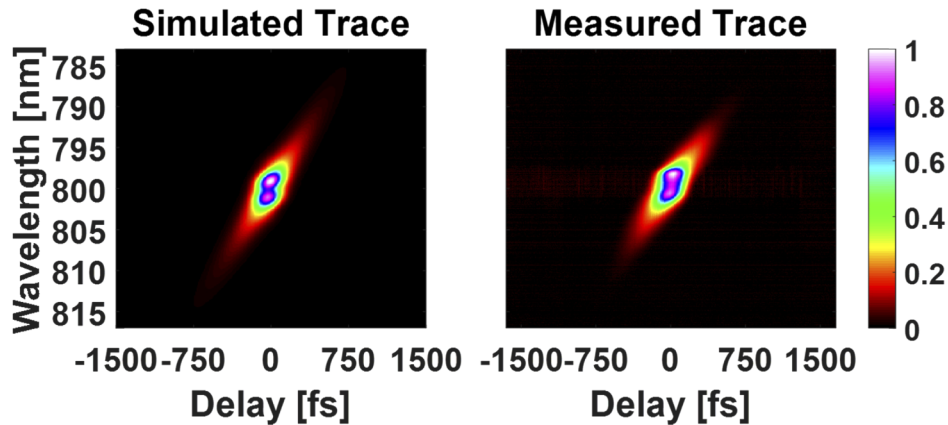


Fig. 3. Simulated trace amplitude (left) and measured trace amplitude (right) for a chirped pulse. Simulation was generated using $E_{ref}(t)$ and $R(t)$ as described in the text.

3.3. IG XFROG measurements of UV pulses using an absorbing medium

To illustrate the method described above, we performed two sets of measurements on pulses with known amounts of chirp introduced by propagating the pulses through glass. In the first measurement, 400 nm test pulses were propagated through 20 mm and 50 mm long rods of SF11 glass. These measurements are shown in Figs. 4(a)-(c). We used the modified GP algorithm discussed in section 3.2 to reconstruct $E_{uv}(t)$ from the measured traces. The reconstructed traces along with the retrieved pulses plotted vs. time and wavelength are shown in the 2nd, 3rd, and 4th rows of Fig. 4 respectively. The second set of measurements was made on pulses centered at 267 nm using a 50 mm rod of UV-grade fused silica (UVFS) to introduce chirp. These traces are shown in Figs. 5(a) and 5(e). The reconstructed traces along with the retrieved pulses plotted vs. time and wavelength are shown in the 2nd, 3rd, and 4th rows of Fig. 5 respectively. In the retrievals shown in Figs. 4 and 5, the G errors (rms difference between the measured and retrieved trace intensities) [8] for each reconstruction were all below 1% indicating convergence [8]. For each measurement, the raw trace was binned to a 128×128 array prior to running the phase-retrieval algorithm.

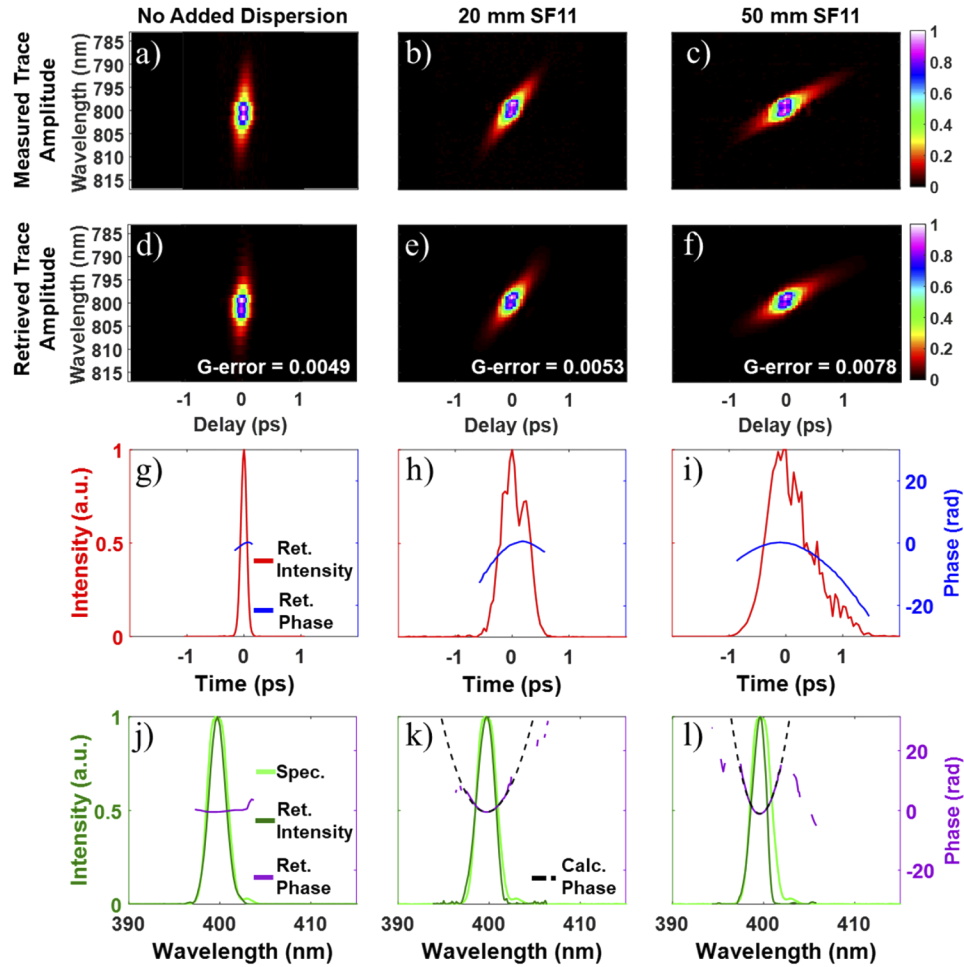


Fig. 4. Measurements of chirped 400 nm pulses using an 800 nm reference pulse. The columns correspond to no added dispersion (left) and dispersion introduced via propagation through 20 mm (center), and 50 mm (right) of SF11. (a-c) Measured Traces. Measured traces were binned to 128×128 arrays. (d-f) Retrieved Traces. (g-i) Temporal intensity (red) and phase (blue) of the retrieved pulse. (j-l) Independently measured spectra (light green), retrieved spectra (dark green), retrieved spectral phase (purple), expected spectral phase calculated from the Sellmeier equations for SF11 (dashed black line).

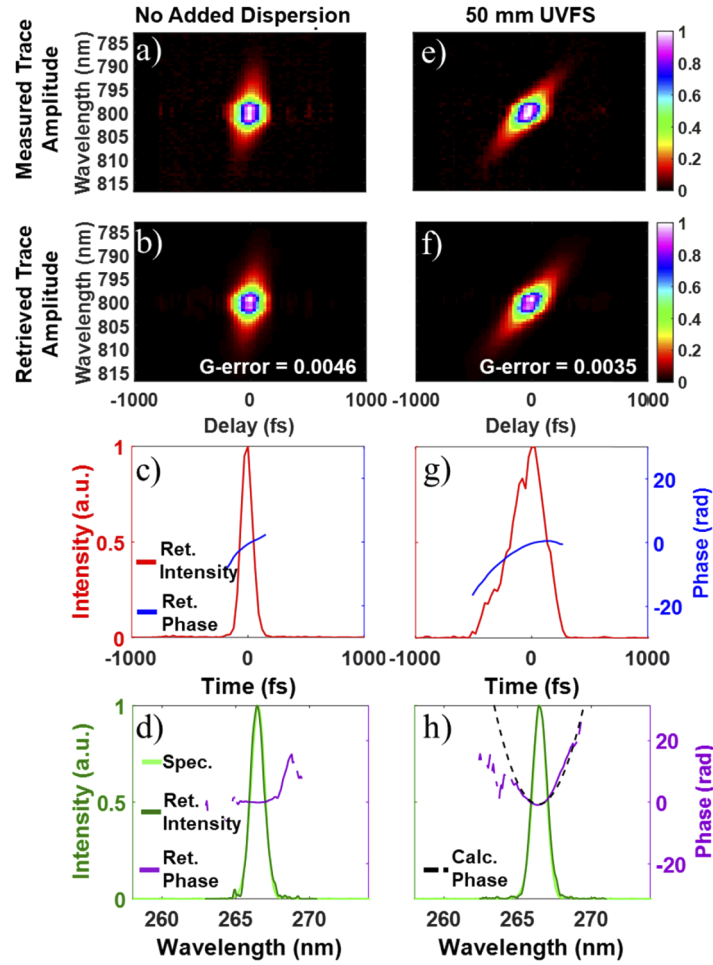


Fig. 5. Measurements of chirped 267 nm pulses using an 800 nm reference pulse. The columns correspond to no added chirp (left) and that with 50 mm (right) of UV-grade fused silica (UVFS). (a) and (e) Measured Traces. Measured traces were binned to 128×128 arrays. (b) and (f) Retrieved Traces. (c) and (g) Temporal intensity (red) and phase (blue) of the retrieved pulse. (d) and (h) Independently measured spectra (light green), retrieved spectra (dark green), retrieved spectral phase (purple), expected spectral phase calculated from the Sellmeier equations for UVFS (dashed black line).

4. Discussion

The measurements presented above demonstrate that a UV femtosecond pulse can be measured using absorption as the nonlinear-optical interaction or time-gate. A key innovation here, is that by measuring the nonlinear signal versus the delay, τ_{uv} , between the pulses making the grating, we significantly reduce the slower incoherent contribution and encode the phase of the UV pulse in the nonlinear signal. This can be understood intuitively by considering that the transient grating is only present when the interfering UV pulses temporally overlap, thus any component of the material response that lasts longer than their interference does not contribute to the nonlinear signal. Figure 2 illustrates this. Figure 2(b) shows a conventional TG measurement where the UV pulses temporally overlap and the reference pulse delay, τ_{ref} , is scanned, which primarily probes the relaxation of the grating. The nonlinear signal versus the grating-pulse-pair delay, τ_{uv} much more closely resembles the measurement made in an instantaneously-responding medium, which is shown for comparison in Fig. 2(d) (as also seen in [28]). The initial rise in the reference scan in Fig. 2(b) contains the UV and NIR temporal profiles, which could be extracted with a deconvolution [29], however this signal does not contain the phase of the UV pulse, only its intensity.

The tilt seen in the measurements in Figs. 4 and 5 clearly demonstrates sensitivity to the phase of the unknown UV pulses. The chirp, which we introduced with the glass rods, causes the redder colors to arrive before the bluer colors. More chirp resulted in more tilt. On top of the tilted component, there is a central region of the trace which remains unchanged when chirp is added; this is the non-phase-containing contribution discussed in sections 3.1 and 3.2 that we included in our model via the step function, due to the fact that some decoherence happens within the pulse duration [24–27]. Note that it was important to set the delay of the reference pulse to zero to maximize the phase-containing contribution. We found that performing a scan of τ_{ref} as shown in Fig. 2(b), and then selecting the reference pulse delay that maximized the bandwidth of the nonlinear signal, was a good approach for finding zero delay.

Applying the phase-retrieval algorithm discussed in section 3.2 to the measured IG XFROG traces further confirms that the pulses can be measured in an absorbing medium, and that the simple model in Eqs. (1) and (2) sufficiently captures the material response for this purpose. The reconstructed traces from each retrieval are shown in the second row of Figs. 4 and 5. The G errors of $< 1\%$, indicate convergence of the algorithm [8]. The full-width-half-maximum temporal widths of the retrieved pulses in Figs. 4(g)-(i) and Figs. 5(c) and 5(g) are approximately 121 fs, 537 fs, and 936 fs, and 119 fs and 316 fs respectively. In Figs. 4(j)-(l) and Figs. 5(d) and 5(h), we compare the retrieved pulse spectrum (dark green) to an independent measurement of the pulse spectrum (light green) made using an Ocean Optics spectrometer, showing relatively good agreement. We also confirmed accurate retrievals by calculating the group delay dispersion (GDD) introduced using the Sellmeier equations for SF11 [30] and UVFS [31], plotted as dashed black lines in Figs. 4(k)-(l) and Fig. 5(h). As seen from a comparison of the retrieved and calculated curves shown in Figs. 4 and 5, the calculated values are in good agreement with the retrieved spectral phases (purple). The retrieved GDDs for the two chirped 400 nm pulses were found to be about 19,470 fs² and 44,978 fs², in good agreement with the calculated values of 17,813 fs² and 44,577 fs². For the chirped 267 nm pulse, the retrieved GDD was found to be 10,657 fs², also in good agreement with the calculated value of 9,826 fs². Minor discrepancies could be due to inaccuracies in the lengths of the glass rods used to introduce the chirp, for example if the rods were slightly tilted, or to the Sellmeier equations used for the calculations not being a perfect match for the rods used in our measurements. Nonetheless, the agreement between the calculated and retrieved phases are within $\sim 10\%$ and suggest that we have accurately extracted the spectral phase using IG XFROG in a slowly responding medium. Comparison to the measurements in Ref. [20], where the same chirped 400 nm pulses were measured, also confirms the accuracy of this technique.

The modulation seen in the FROG traces was confirmed to be from a weak post pulse in the reference pulse that occurred ~ 850 fs after the main pulse, as mentioned in Section 2. The long-lived grating in ZnS results in contributions to the nonlinear signal over a broad time-window, so that the weak post pulse in the reference also contributes to the nonlinear signal. Since we were not able to experimentally remove this artifact, incorporating the post pulse into our reference pulse shape as a weak replica of the main pulse improved the accuracy of the IG XFROG retrievals.

In all of the measurements reported here, we used a fluence of < 10 mJ/cm². We expect that lower fluences would also be sufficient by using a longer integration time on the camera. While the nonlinear medium used in the measurements presented here was ZnS, which is completely opaque at 267, but has a transmittance of ~ 50 -55% at 400 nm [32], we expect that the measurements would work similarly (perhaps with some adjustment to $R(t)$) with any medium that is absorbing at the unknown pulse wavelength but transparent at the probe wavelength. Moreover, we estimate the groove density of our induced gratings to be about 98 and 150 grooves/mm for the 267 nm and 400 nm measurements respectively. The angular dispersion produced by such low-density gratings is small and did not interfere with the collection of the nonlinear signal in the measurements presented here. In the case of non-negligible angular dispersion from the induced grating (e.g. if a spectrally broader reference pulse is used), imaging the sample onto the detector and spectrally dispersing the signal in the perpendicular dimension should alleviate any effects. Also, because the phase-matching bandwidth of this technique is relatively broad ($> \sim 100$ nm here), shorter pulses should also be measureable with this technique. The phase-matching bandwidth can be increased, if need be, by changing the beam size and the focal length of the optics used to focus the beams onto the nonlinear medium (see [20,21]).

Here, we used a spectrally narrow and relatively long duration reference pulse (~ 400 fs) because this made it easier to visually see the tilt in the spectrograms due to the phase of the UV pulse. This is not a requirement, but is convenient for quick intuitive visual feedback from the measurement (similar to XFROG [8]). Having performed a number of simulations with different reference pulse durations, we find that IG XFROG works well for reference pulses that are shorter or longer than the unknown pulse, placing no strict requirements on its duration; it just needs to be characterized. Similar to standard XFROG, we recommend, when possible, to use a simple reference pulse that is at least close in duration to the unknown pulse, to avoid introducing unnecessary spectral or temporal complexity into the measurement and spectrogram [8]. Finally, we point out that IG XFROG measurements are not very sensitive to errors in the reference pulse, since the reference pulse is encoded in the trace differently than the unknown pulse (again similar to standard XFROG [33]). As shown in Supplement 1, relatively large amounts of chirp can be added to the reference pulse with minimal changes in the spectrograms.

An interesting direction for future work could be to develop an algorithm that extracts both the UV pulse and the medium's response function, similar to the double blind-FROG approach [8,33]. Another option could be to extract the material response from a reference scan [15,29]. Nevertheless, the measurements provided here indicate that the simple model in Eqs. (1) and (2) is sufficient for most applications, and this approach has the major advantage of being easy and fast to implement in the phase-retrieval algorithm.

5. Conclusion

In summary, we presented proof-of-principle measurements which demonstrate IG XFROG's ability to measure UV pulses using band-gap absorption as the nonlinear-optical time-gate. We show that, by scanning the delay between the two UV pulses, IG XFROG selectively detects the instantaneous, phase-preserving contribution to the nonlinear signal; the initial, fast part of the photoexcitation where the light remains coherent with the photoexcited electrons. We presented a simple model for the response of the medium and incorporated this model into a modified GP

phase-retrieval algorithm. We used this algorithm to retrieve chirped UV pulses centered at 400 nm and 267 nm from experimentally measured traces and showed that accurate measurements of the pulse spectral phase are obtained. While we demonstrated this method at 400 and 267 nm, the process of absorption, whether it is across the bandgap or into the continuum, (i.e. photoionization) is not strongly dependent on wavelength. Thus, we expect IG XFROG to be applicable deeper into the UV and possibly even at x-ray energies. Moreover, like other versions of FROG [8], single-shot IG XFROG measurements should also be feasible [34], potentially providing access to single-shot optical-read-out pulse measurement from the UV into the x-ray range.

Funding. Laboratory Directed Research and Development (20180242ER); Los Alamos National Laboratory (African-American Partnership Program); National Science Foundation (ECCS-1609808); Georgia Research Alliance.

Acknowledgments. This work was performed, in part, at the Center for Integrated Nanotechnologies, an Office of Science User Facility operated for the U.S. Department of Energy (DOE) Office of Science. The Los Alamos National Laboratory, an affirmative action equal opportunity employer, is managed by Triad National Security, LLC for the U.S. Department of Energy's NNSA, under Contract No.89233218CNA000001.

Disclosures. Rick Trebino owns a company that sells pulse-measurement devices.

Supplemental document. See [Supplement 1](#) for supporting content.

References

1. T. Brabec and F. Krausz, "Intense few-cycle laser fields: Frontiers of nonlinear optics," *Rev. Mod. Phys.* **72**(2), 545–591 (2000).
2. E. Allaria, R. Appio, L. Badano, W. A. Barletta, S. Bassanese, S. G. Biedron, A. Borgia, E. Busetto, D. Castronovo, P. Cinquegrana, S. Cleva, D. Cocco, M. Cornacchia, P. Craievich, I. Cudin, G. D'Auria, M. Dal Forno, M. B. Danailov, R. De Monte, G. De Nino, P. Delgiusto, A. Demidovich, S. Di Mitri, B. Diviacco, A. Fabris, R. Fabris, W. Fawley, M. Ferianis, E. Ferrari, S. Ferry, L. Froehlich, P. Furlan, G. Gaio, F. Gelmetti, L. Giannessi, M. Giannini, R. Gobessi, R. Ivanov, E. Karantzoulis, M. Lanza, A. Lutman, B. Mahieu, M. Milloch, S. V. Milton, M. Musardo, I. Nikolov, S. Noe, F. Parmigiani, G. Penco, M. Petronio, L. Pivetta, M. Predonzani, F. Rossi, L. Rumiz, A. Salom, C. Scafuri, C. Serpico, P. Sigalotti, S. Spampinati, C. Spezzani, M. Svandrlik, C. Svetina, S. Tazzari, M. Trovo, R. Umer, A. Vascotto, M. Veronese, R. Visintini, M. Zaccaria, D. Zangrando, and M. Zangrando, "Highly coherent and stable pulses from the FERMI seeded free-electron laser in the extreme ultraviolet," *Nat. Photonics* **6**(10), 699–704 (2012).
3. K. Tiedtke, A. Azima, N. Von Bargen, L. Bittner, S. Bonfigt, S. Düsterer, B. Faatz, U. Fröhling, M. Gensch, and C. Gerth, "The soft x-ray free-electron laser FLASH at DESY: beamlines, diagnostics and end-stations," *New J. Phys.* **11**(2), 023029 (2009).
4. F. Krausz and M. Ivanov, "Attosecond physics," *Rev. Mod. Phys.* **81**(1), 163–234 (2009).
5. K. Ramasesha, S. R. Leone, and D. M. Neumark, "Real-time probing of electron dynamics using attosecond time-resolved spectroscopy," *Annu. Rev. Phys. Chem.* **67**(1), 41–63 (2016).
6. E. T. J. Nibbering, H. Fidder, and E. Pines, "ULTRAFast CHEMISTRY: Using Time-Resolved Vibrational Spectroscopy for Interrogation of Structural Dynamics," *Annu. Rev. Phys. Chem.* **56**(1), 337–367 (2005).
7. D. F. Gardner, M. Tanksalvala, E. R. Shanblatt, X. Zhang, B. R. Galloway, C. L. Porter, R. Karl Jr, C. Bevis, D. E. Adams, H. C. Kapteyn, M. M. Murnane, and G. F. Mancini, "Subwavelength coherent imaging of periodic samples using a 13.5 nm tabletop high-harmonic light source," *Nat. Photonics* **11**(4), 259–263 (2017).
8. R. Trebino, *Frequency-Resolved Optical Gating: The Measurement of Ultrashort Laser Pulses*, 1 ed. (Springer, 2002).
9. M. Rhodes, G. Steinmeyer, J. Ratner, and R. Trebino, "Pulse-shape instabilities and their measurement," *Laser Photonics Rev.* **7**(4), 557–565 (2013).
10. R. Jafari and R. Trebino, "Extremely Robust Pulse Retrieval From Even Noisy Second-Harmonic-Generation Frequency-Resolved Optical Gating Traces," *IEEE J. Quantum Electron.* **56**(1), 1–8 (2020).
11. R. Jafari and R. Trebino, "Highly Reliable Frequency-Resolved Optical Gating Pulse-Retrieval Algorithmic Approach," *IEEE J. Quantum Electron.* **55**(4), 1–7 (2019).
12. P. Sidorenko, O. Lahav, Z. Avnat, and O. Cohen, "Ptychographic reconstruction algorithm for frequency-resolved optical gating: super-resolution and supreme robustness," *Optica* **3**(12), 1320–1330 (2016).
13. T. Zahavy, A. Dikopoltsev, D. Moss, G. I. Haham, O. Cohen, S. Mannor, and M. Segev, "Deep learning reconstruction of ultrashort pulses," *Optica* **5**(5), 666–673 (2018).
14. K. W. DeLong, C. L. Ladera, R. Trebino, B. Kohler, and K. R. Wilson, "Ultrashort-pulse measurement using noninstantaneous nonlinearities: Raman effects in frequency-resolved optical gating," *Opt. Lett.* **20**(5), 486–488 (1995).
15. A. Leblanc, P. Lassonde, S. Petit, J. C. Delagnes, E. Haddad, G. Ernotte, M. R. Bionta, V. Gruson, B. E. Schmidt, H. Ibrahim, E. Cormier, and F. Legare, "Phase-matching-free pulse retrieval based on transient absorption in solids," *Opt. Express* **27**(20), 28998–29015 (2019).

16. R. Itakura, T. Kumada, M. Nakano, and H. Akagi, "Frequency-resolved optical gating for characterization of VUV pulses using ultrafast plasma mirror switching," *Opt. Express* **23**(9), 10914–10924 (2015).
17. R. P. Prasankumar and A. J. Taylor, *Optical techniques for solid-state materials characterization* (CRC, 2016).
18. Y. Mairesse and F. Quéré, "Frequency-resolved optical gating for complete reconstruction of attosecond bursts," *Phys. Rev. A* **71**(1), 011401 (2005).
19. J. Itatani, F. Quéré, G. L. Yudin, M. Y. Ivanov, F. Krausz, and P. B. Corkum, "Attosecond Streak Camera," *Phys. Rev. Lett.* **88**(17), 173903 (2002).
20. T. Jones, W. K. Peters, A. Efimov, R. L. Sandberg, D. Yarotski, R. Trebino, and P. Bowlan, "Encoding the complete electric field of an ultraviolet ultrashort laser pulse in a near-infrared nonlinear-optical signal," *Opt. Express* **28**(18), 26850–26860 (2020).
21. D. Lee, P. Gabolde, and R. Trebino, "Toward single-shot measurement of a broadband ultrafast continuum," *J. Opt. Soc. Am. B* **25**(6), A34–A40 (2008).
22. H. Valtina-Lukner, F. Belli, A. Ermolov, F. Kottig, K. F. Mak, F. Tani, J. C. Travers, and P. S. J. Russell, "Extremely broadband single-shot cross-correlation frequency-resolved optical gating using a transient grating as gate and dispersive element," *Rev. Sci. Instrum.* **88**(7), 073106 (2017).
23. R. Boyd, *Nonlinear Optics*, 3rd ed. (Academic, 2008).
24. A. Weiner, *Ultrafast optics* (John Wiley & Sons, 2011).
25. E. Ippen and C. Shank, "Ultrashort light pulses," in *Topics in applied physics*, S. L. Shapiro, ed. (Springer, 1977), p. 83–122.
26. T. Heinz, S. Palfrey, and K. Eisenthal, "Coherent coupling effects in pump-probe measurements with collinear, copropagating beams," *Opt. Lett.* **9**(8), 359–361 (1984).
27. S. Mukamel, *Principles of nonlinear optical spectroscopy* (Oxford University, 1995).
28. F. Capotondi, L. Foglia, M. Kiskinova, C. Masciovecchio, R. Mincigrucci, D. Naumenko, E. Pedersoli, A. Simoncig, and F. Bencivenga, "Characterization of ultrafast free-electron laser pulses using extreme-ultraviolet transient gratings," *J. Synchrotron Radiat.* **25**(1), 32–38 (2018).
29. D. J. Kane, N. Hartmann, R. N. Coffee, and A. R. Fry, "Experimental and analysis considerations for transmission/reflection spectrograms used in ultrafast x-ray pulse diagnostics," *Proc. SPIE* **9740**, 97400H (2016).
30. "RefractiveIndex.INFO: Refractive Index Database, Optical constants of SF11," (2020), retrieved April 1, 2020, <https://refractiveindex.info/?shelf=glass&book=SF11&page=SCHOTT>.
31. "Newlight Photonics Inc., Newlight Photonics: Fused Silica (SiO₂) Windows/Rods," (2020), retrieved July 31, 2020, <https://www.newlightphotonics.com/Optical-Windows-Rods/Fused-Silica-Windows-Rods>.
32. "Edmund Optics Zinc Sulfide Multispectral Windows," (2021), retrieved February 11, 2021, <https://www.edmundoptics.com/f/zinc-sulfide-multispectral-windows/14004/>.
33. T. C. Wong, J. Ratner, V. Chauhan, J. Cohen, P. M. Vaughan, L. Xu, A. Consoli, and R. Trebino, "Simultaneously measuring two ultrashort laser pulses on a single-shot using double-blind frequency-resolved optical gating," *J. Opt. Soc. Am. B* **29**(6), 1237–1244 (2012).
34. W. Peters, T. Jones, A. Efimov, E. Pedersoli, L. Foglia, R. Mincigrucci, I. Nikolov, R. Trebino, R. Sandberg, M. Danailov, F. Capotondi, F. Bencivenga, and P. Bowlan, "Single-shot Measurement of Extreme Ultraviolet Free Electron Laser Pulses," in *Conference on Lasers and Electro-Optics, OSA Technical Digest* (Optical Society of America, 2020), paper FW4D.3.